Cryogenics 149 (2025) 104078

Contents lists available at ScienceDirect

Cryogenics

journal homepage: www.elsevier.com/locate/cryogenics

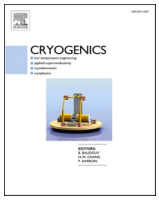

An analytical framework for computing AC losses in the HTS insert of the EU-DEMO central solenoid☆

Gianluca De Marzi [a,*], Valentina Corato [a], Monika Lewandowska [b,c]

[a] Nuclear Department, ENEA, Frascati Research Center, Frascati 00044, Italy
[b] The Henryk Niewodniczański Institute of Nuclear Physics, Polish Academy of Science, Krakow 31-342, Poland
[c] Faculty of Mechanical Engineering and Mechatronics, West Pomeranian University of Technology in Szczecin, 70-310, Poland

ARTICLE INFO

Keywords:
EU DEMO
Ac loss
Superconducting magnets
Numerical simulations
Electromagnetic analysis
Coupling loss

ABSTRACT

High-temperature superconductors (HTS) are being explored for integration into coil systems for magnetic confinement fusion, due to their ability to extend operational margins in terms of temperature, current, and magnetic field. Recently, a conductor design based on a sector-assembled (SECAS) cable-in-conduit-conductor (CICC) concept was proposed for the innermost layer of the central solenoid (CS) module in the EU-DEMO tokamak. The dynamic nature of plasma scenarios, characterized by rapid variations in current and magnetic fields, induces significant AC losses in the superconducting magnets. These losses can be particularly pronounced during phases like plasma start-up and control operation, where field variations can be significant. In this study, we evaluate the instantaneous power losses — both hysteretic and coupling losses — during a baseline plasma scenario using an analytical model that accurately accounts for the temporal evolution of the magnetic field profile within the innermost layers of the CS1 HTS insert.

1. Introduction

The magnetic systems in various new magnetic confinement fusion projects, which are rapidly advancing in both the public and private sectors, rely on high-temperature superconductors (HTS) [1].

Thanks to their ability to generate higher magnetic fields, HTS-based tokamaks could offer significant advantages, such as the potential for more compact machines with reduced construction times [2].

The EUROfusion Consortium is currently investigating the integration of HTS technology into EU-DEMO, the planned European fusion reactor [3–5]. For the central solenoid, a hybrid solution has been proposed, combining HTS, Nb_3Sn, and NbTi conductors for the high-, medium-, and low-field sections, respectively [3]. This hybrid approach offers promising benefits, such as the potential to reduce the solenoid's outer radius and thereby the overall size and cost of the tokamak, or to enhance the generated magnetic flux, extending the plasma burn duration.

To sustain the required magnetic flux, the HTS insert conductor in the central solenoid must operate stably at 4.5 K, withstanding currents up to 60 kA and magnetic fields up to 18 T [6] and maintaining performance for 20,000 plasma cycles. Toward this end, a novel sector-based HTS cable concept has been proposed, referred to as the SECtor-ASsembled cable (SECAS), see Fig. 1. This concept relies on units formed by braided stacks of superconducting tapes (BRAST), which facilitate effective handling and optimal protection of the tapes throughout the cable fabrication process. Given the performance capabilities of commercial conductors, achieving the specified requirements of 60 kA and 18 T requires 180 tapes of 4 mm width.

In this work, we applied an analytical method [[7] to evaluate the losses occurring in the HTS insert of the EU-DEMO central solenoid under a reference plasma scenario.

2. Methodology

2.1. Geometrical and operational requirements

The geometric and operational requirements for the EU DEMO magnet design are based on output provided by the reactor systems code PROCESS [8,9]. The current reference for magnet design is the 2018 Baseline [3], which assumes a free-standing CS coil situated within the bore formed by 16 wedged Toroidal Field (TF) coils. The solenoid is divided into five electrically independent modules to enable plasma

☆ This article is part of a special issue entitled: 'SPAS-2024' published in Cryogenics.

* Corresponding author.
E-mail address: gianluca.demarzi@enea.it (G.D. Marzi).

https://doi.org/10.1016/j.cryogenics.2025.104078
Received 6 February 2025; Received in revised form 3 April 2025; Accepted 11 April 2025
Available online 19 April 2025
0011-2275/© 2025 The Authors. Published by Elsevier Ltd. This is an open access article under the CC BY license (http://creativecommons.org/licenses/by/4.0/).

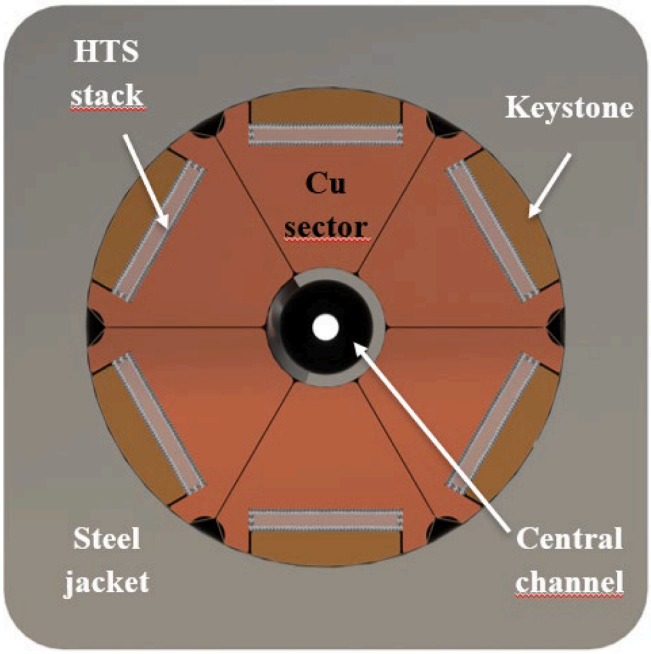

Fig. 1. Cross-section of the sector-shaped HTS cable designed by ENEA.

shaping control.

The winding pack layout of the CS DEMO graded design proposed by Swiss Plasma Center [3] is illustrated in Fig. 2. In this graded-layer design, the dimensions of turns change from layer to layer. This graded design includes the HTS superconductor in the innermost double-layer sub-coil, react-and-wind Nb_3Sn in the medium-field sub-coils, and NbTi in the three outermost sub-coils. The proposed cable-in-conduit-conductors (CICCs) use rectangular steel conduits as structural material.

The equilibrium currents for the coils are specified at three key instants during the CS magnetic flux swing: pre-magnetization (Pre-mag), start-of-flat top (SOF), and end-of-flat top (EOF). The highest magnetic field and mechanical stresses in the solenoid occur during the pre-mag.

The geometric parameters are summarized in Table 1, whereas the current scenarios used are reported in Table 2.

Table 1
Coil coordinates and dimensions.

Coil ID	R [m]	Z [m]	ΔR [m]	ΔZ [m]
CS3U	2.1104	7.0505	1.1808	2.86330
CS2U	2.1104	4.0375	1.1808	2.8630
CS1	2.1104	−0.3990	1.1808	5.7100
CS2L	2.1104	−4.8355	1.1808	2.8630
CS3L	2.1104	−7.8485	1.1808	2.8630
PF1	5.4000	9.6600	1.1500	1.1500
PF2	14.0000	7.9000	0.8500	0.8500
PF3	17.9700	2.5000	1.1000	1.1000
PF4	17.9700	−2.5000	1.1000	1.1000
PF5	14.0000	−7.9000	1.2000	1.2000
PF6	7.0000	−10.6000	1.4000	1.4000

Table 2
Current scenario.

Current [MA]	Pre-Mag	SOF	EOF
CS3U	36.12	16.91	−7.37
CS2U	36.12	−1.76	−36.11
CS1	72.24	−11.91	−72.24
CS2L	36.12	−8.9	−36.11
CS3L	34.89	31.19	−15.43
PF1	20.51	17.6	2.88
PF2	4.79	−6.48	−7.31
PF3	−10.51	−6.35	−7.54
PF4	14.92	−4.94	−4.52
PF5	−12.3	−9.63	−11.14
PF6	29.81	19.18	12.72
Plasma	0	17.86	17.86

2.2. Electromagnetic analysis

A parametric electromagnetic model of the DEMO magnet system was developed in Comsol Multiphysics [10] using the *magnetic fields interface* (mf) of the AC/DC module. The physics interface solves Maxwell's equations, which are formulated using the magnetic vector potential as the dependent variables.

The toroidal-field coils were excluded from the analysis, given their negligible influence on the magnetic field at the inner bore where the CS is located. An example of a field map generated by the finite element software is shown in Fig. 3.

The whole field cycle of the poloidal magnetic field comprises the following phases: (i) conductor current ramp-up to the pre-mag level (500 s); (ii) plasma current ramp-up (PCRU, 100 s), which ends at SOF; (iii) plasma burn (7200 s, between the SOF and the EOF); (iv) conductor current ramp-down, between the EOF and the end-of-plasma, EOP (CRD, 100 s); and dwell time (600 s).

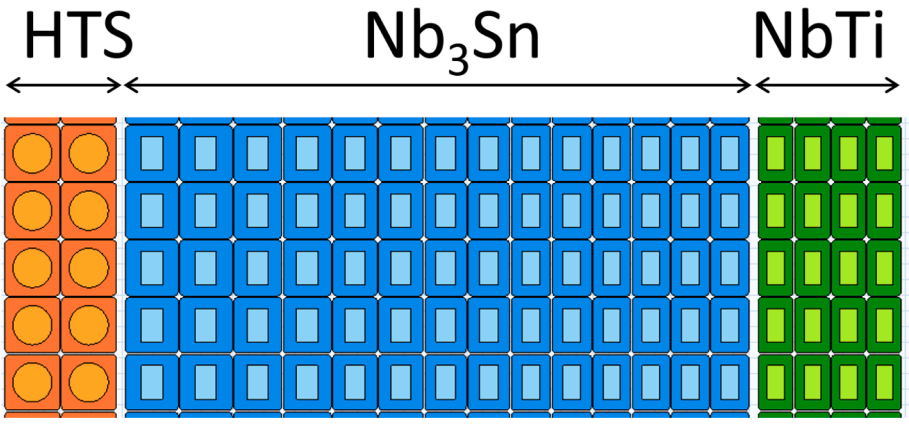

Fig. 2. Radial slice showing five rows of conductors of the CS1 hybrid design. Orange: high-field grade (HTS); blue: mid-field grade (Nb3Sn); and green: low-field grade (NbTi). (For interpretation of the references to colour in this figure legend, the reader is referred to the web version of this article.)

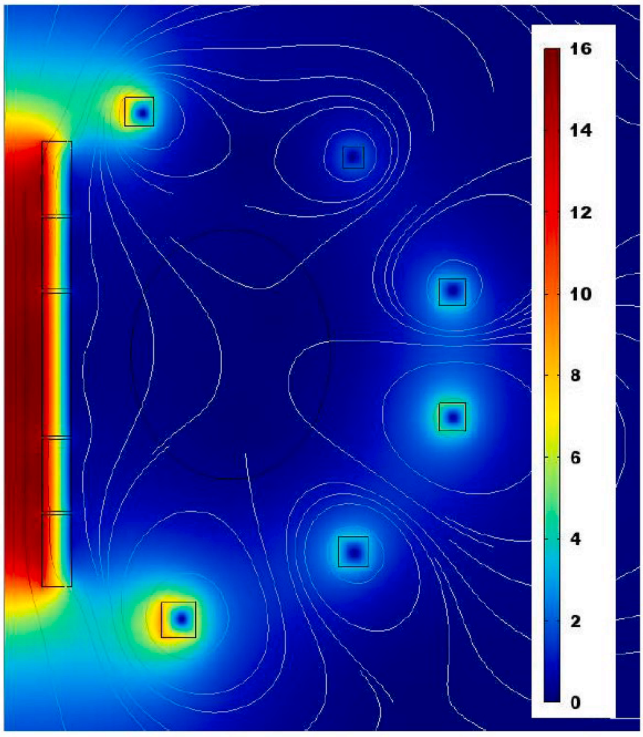

Fig. 3. Map of the poloidal component of the magnetic field at Pre-Mag.

3. Modelling of AC losses

3.1. Magnetization loss

Recently, we have developed an analytical model to evaluate the power losses in HTS twisted stacked cables [7]. This model accurately predicts instantaneous power losses in cables composed of a limited number of tapes per stack, providing sufficient precision for high-field conditions.

The instantaneous power loss density of a twisted cable due to the hysteresis, P_{magn}, is determined as the average value over one twist pitch, obtained by integrating the sum of the two components P_{slab} and P_{strip} arising from the perpendicular ($B_{e\perp}$) and parallel ($B_{e\|}$) components of the external field B_e:

$$P_{magn}\left[\frac{W}{m^3}\right] = \frac{2}{\pi}\int_0^{\frac{\pi}{2}} \left[P_{slab}(B_{e\|}) + P_{strip}(B_{e\perp})\right] d\theta \tag{1}$$

In the absence of transport current, the analytical expressions for the magnetization loss during the initial energization from the virgin state (with no trapped field at the start of the ramp-up) are as follows:

$$P_{slab} = \frac{B_p^2}{2\mu_0}\partial_t B_{e\|}\begin{cases}\dfrac{B_{e\|}^2}{B_p^3} & B_e \le B_p \\ \dfrac{1}{B_p} & B_e \ge B_p\end{cases} \tag{2}$$

$$P_{strip} = \frac{1}{4}J_c w \partial_t B_{e\perp}\left[\tanh\left(\frac{B_{e\perp}}{B_c}\right) - \frac{B_{e\perp}}{B_c}\mathrm{sech}^2\left(\frac{B_{e\perp}}{B_c}\right)\right]\partial_t B_{e\perp} \tag{3}$$

where $\partial_t B_e$ represents the time derivative of the external field (parallel or perpendicular component), $B_p = \mu_0 J_c d/2$ is the full penetration field for a single tape, J_c is the critical current density, d is the thickness of the superconducting layer, $B_c = \mu_0 J_c d/\pi N$, N is the number of tapes in each HTS stack, and w is the width of the thin strip. The calculation of AC losses in the HTS insert is based on the critical surface properties of REBCO tapes, as described in [7]. Specifically, the model accounts for the dependence of the critical current on both the magnitude and orientation of the local magnetic field, following the extended Kim model.

The previous formulas apply to the initial ramp-up, from zero to the maximum B_{em}. However, when the field, after reaching its maximum, decreases to zero and then rises again (without exceeding B_{em}) – corresponding to the PCRU and burn phases – the formulas to be used are:

$$P_{slab} = \frac{B_p^2}{2\mu_0}|\partial_t B_{e\|}|\begin{cases}\dfrac{(B_{em} + \mathrm{sgn}(\partial_t B_{e\|})B_e)^2}{4B_p^3} & \mathrm{sgn}(\partial_t B_{e\|})B_e \le 2B_p - B_{em\|} \\ \dfrac{1}{B_p} & \mathrm{sgn}(\partial_t B_{e\|})B_e \ge 2B_p - B_{em\|}\end{cases} \tag{4}$$

$$P_{strip} = \frac{1}{4}J_c w\left[\tanh(\xi) - \xi\mathrm{sech}^2(\xi)\right]|\partial_t B_{e\perp}| \; with \; \xi = \frac{B_{em\perp} + \mathrm{sgn}(\partial_t B_{e\perp})B_{e\perp}}{2B_c} \tag{5}$$

In this study, we apply this analytical approach to assess the AC losses generated in a simplified DEMO plasma scenario. To quantify B_e, we calculated the magnetic field at six distinct points within the CS1 insert, as illustrated in Fig. 4. Since this insert is located at the center of the CS and in its innermost region, the field variations across the six points are minimal. As an additional simplification, we therefore used a single $B_e(t)$ profile, defined as the average of the magnetic field calculated at the six points in CS1.

Due to the multi-slot configuration of the SECAS cable, in (1) we can neglect the contribution from the parallel component of the field. In fact, this component can be disregarded unless the external field is almost perfectly aligned with the flat surface of the tapes [7]. Now, regardless of which section of the cable length is considered, the twist ensures that at least four stacks are never perfectly aligned with the external field. Therefore, (1) can be further simplified using the expression:

$$P_{magn}\left[\frac{W}{m^3}\right] = \frac{2}{\pi}\int_0^{\frac{\pi}{2}} P_{strip}(B_{e\perp})d\theta \tag{6}$$

3.2. Coupling loss

The coupling losses result from induced currents flowing both within tapes in the same stack and between different stacks. Coupling loss models have been developed in the past for low-temperature-superconducting (LTS) CICCs [11–13]. Although HTS cables differ from their LTS counterparts in various aspects, in this analysis we applied coupling loss theory to the SECAS conductor under examination. The coupling loss power density per unit volume depends on the square of the local field variation $\partial_t B_i$, i.e. the "internal" applied field after accounting for the coupling current shielding [11]:

$$P_{coupling}\left[\frac{W}{m^3}\right] = \frac{(\partial_t B_i)^2}{\rho_{et}}\left(\frac{l_p}{2\pi}\right)^2 = \frac{2(\partial_t B_i)^2}{\mu_0}\tau \tag{7}$$

The coupling loss time constant, τ, which provides an indication of the relaxation time of the coupling currents, can be expressed in terms of an effective transverse resistivity ρ_{et} and the cable twist pitch l_p as:

$$\tau = \frac{\mu_0}{2\rho_{et}}\left(\frac{l_p}{2\pi}\right)^2 \tag{8}$$

The temporal behavior of $\partial_t B_i$ is obtained from the externally applied field $B_e(t)$ by solving the ordinary differential equation $B_e - B_i = \tau\partial_t B_i$ [14]. Here, it is calculated iteratively using a forward finite-difference method with constant temporal spacing.

As in [15], we assume a linear dependence on the applied external field: $\tau = \tau_0\ t\ \tau_1 B_e$, where τ_0 represents the value at zero field and τ_1

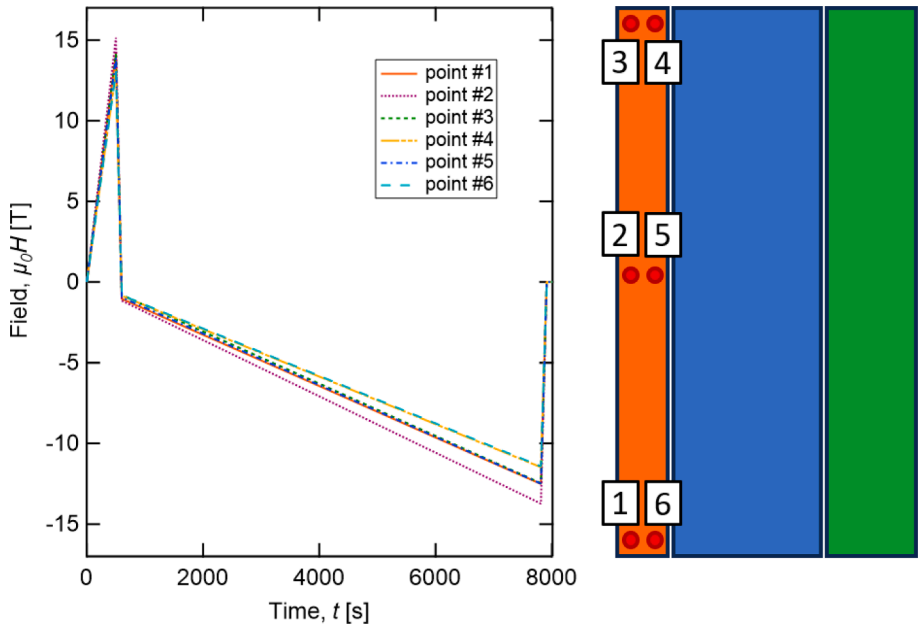

Fig. 4. Evolution of the external field during the plasma scenario, calculated at selected points of the CS1 module of the CS1 insert. Right: schematization of the CS1 module, not in scale. Orange: high-field grade (HTS); blue: mid-field grade (Nb_3Sn); and green: low-field grade (NbTi). (For interpretation of the references to colour in this figure legend, the reader is referred to the web version of this article.)

denotes the slope. The coupling loss parameters τ_0 and τ_1 have been approximately based on the values derived from the ITER CS Insert (CSI) test campaign and the factory testing of the first two CS modules (CSM1&2) [16]: $\tau_0 = 300$ ms; and $\tau_1 = -0.018$ s/T. These parameters are to be considered indicative, as they could vary substantially in the actual SECAS cable, especially τ_0. Unfortunately, no experimental parameters are currently available for the SECAS cable that would permit a more accurate estimation of the coupling time constant.

As part of our modeling, we considered the eddy and coupling current losses in the Cu sectors, which can be divided into intra-sector and inter-sector losses. The intra-sector losses can be neglected, as the associated time constants are on the order of a few milliseconds [17], significantly lower than those of inter-sector losses, which are expected to be in the range of hundreds of milliseconds. This topic is currently under investigation, and we are developing a dedicated FEM model to better estimate τ for SECAS cables. While no experimental measurements are available at the moment, future efforts will aim at setting up a dedicated test campaign. A more detailed analysis will be presented in a forthcoming publication.

Fig. 5 shows the evolution of τ during the plasma scenario considered in this article.

3.3. In-field critical current

For the description of the in-field and angular dependence of the critical current of the HTS tapes, $I_c(B,\theta)$, we have considered an extended version of the conventional Kim model [18,19]:

$$I_c(B,\theta) = \frac{I_{c0}}{\left[1 + \varepsilon(\theta)\left(\frac{B}{B_0}\right)^{\alpha}\right]^{\beta}} \tag{9}$$

Here, the anisotropy function is defined as $\varepsilon(\theta) = \sqrt{\gamma^{-2}\sin^2(\theta) + \cos^2(\theta)}$, in which $\gamma = 5$ [20] is the anisotropy factor, and θ represents the angle between the field and the normal to the flat surface of the tapes. The empirical parameters have been obtained by fitting to the experimental data [7]: $I_{c0} = 4$ kA for a 4-mm width tape, $\alpha = 0.54$, $\beta = 2.18$, and $B_0 = 5.72$ T.

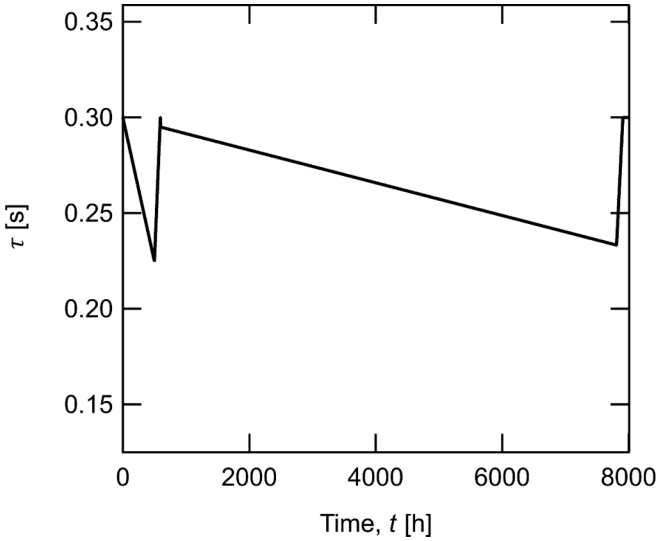

Fig. 5. Evolution of the time coupling constant, τ, during the DEMO plasma scenario described in the text. For reference, we used the simple linear equation described in [15]: $\tau(t) = \tau_0 + \tau_1 B_e(t)$, with $\tau_0 = 300$ ms and $\tau_1 = -0.018$ s/T.

4. Results

In this work, we considered the cable layout corresponding to Option-C as described in [7]. In such configuration, each sector contains six BRASTs, where each BRAST consists of five 4-mm-wide tapes. This results in a total of 36 BRASTs and 180 tapes.

The evolution of the instantaneous losses, expressed in W/m, due to both magnetization and coupling currents is shown in Fig. 6. For convenience, the internal field $B_i(t)$ is also plotted on the same graph.

As can be seen, the magnetization losses are consistently higher than those due to the coupling currents. During the burn phase, the ratio is approximately 500, while during the PCRU and CRD phases, the factor varies between 2 and 5. In the initial magnet charging phase, up to premag, the ratio is around 10.

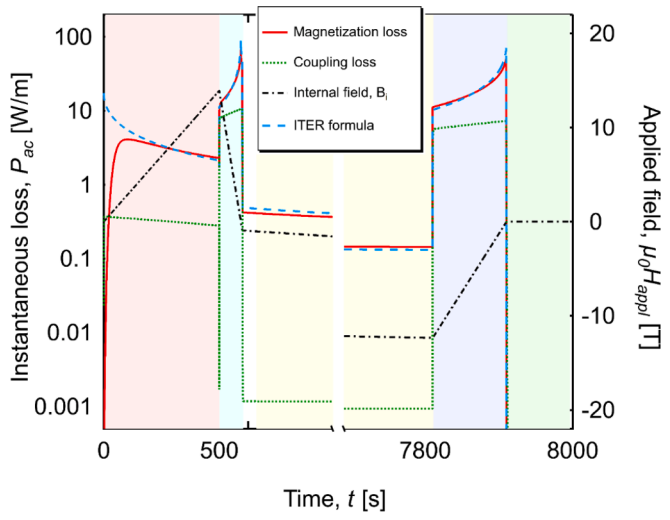

Fig. 6. The behaviour of the magnetization loss (red continuous line), coupling loss (green dotted line) and internal field Bi(t) (black dotted-and-dashed line) as a function of time during the DEMO plasma scenario described in the text. The magnetization loss calculated using the ITER formula is also plotted as a blue dashed line. (For interpretation of the references to colour in this figure legend, the reader is referred to the web version of this article.)

It should be noted that the coupling losses might be underestimated due to the reasons outlined earlier. Nonetheless, a direct approach to further reduce these losses, particularly during the pre-mag, PCRU, and CRD phases, is to decrease the ramp-rate. However, during the breakdown phase (first 1–2 s after pre-mag), it is necessary to maintain a high ramp-rate for the plasma start-up. This means that coupling losses could potentially exceed hysteresis losses in this phase. The breakdown process is still under development, and further detailed studies will be required to better understand and optimize this phase.

The case is different for magnetization losses. A key strategy for reducing these losses is primarily to modify the aspect ratio of the superconducting tapes [21,22]. By modifying the aspect ratio of the conductor, it is possible to control the losses more effectively. Another possible alternative for reducing losses is to striate the tape to create filaments [23–25]. The use of striated tapes can also be considered a valid solution for loss mitigation in fusion cables operating under high-field conditions.

The dissipated power over the entire cycle was determined by integrating the curves shown in Fig. 6 over time, yielding values of 7.32 kJ/m for magnetization losses and 1.74 kJ/m for coupling losses. Magnetization losses are approximately 4.2 times higher than coupling losses, and as such, remain notably high, representing a significant technological barrier to the implementation of HTS in magnets for nuclear fusion applications.

It is also interesting to perform the calculation using the formulas previously employed for LTS conductors, as in the ITER project [15]. In this context, the formula used to calculate the instantaneous power loss when the superconductor is fully penetrated is:

$$P_{LTS} = \frac{2}{3\pi} J_c d_{eff} |\partial_t B_e| \tag{10}$$

In Equation (10), the effective diameter d_{eff} is replaced by the tape width, and the critical current density is evaluated at $\theta = 0$. The integrated power loss dissipated over the entire cycle is 8.26 kJ/m, which is 112.84 % of the 7.32 kJ/m obtained with Eq. (6). Despite the approximations made, the agreement with the results obtained using (10) is more than satisfactory. In other words, this result suggests that the tape stack behaves like a multifilamentary composite, where the filaments have a diameter equal to the tape width. This finding also provides a direct explanation for why the losses in HTS conductors are much higher than in LTS conductors.

The losses obtained with the formula for LTS are slightly higher because the conductor was assumed to be fully penetrated at all times. As shown in Fig. 6, it is evident that, for example, during the energization phase of the coils, equation (10) significantly overestimates the losses.

To further strengthen this point, a comparison with AC losses estimated for the ITER central solenoid [26] indicates that, after adjusting for differences in burn-time and volume, the AC losses in a single DEMO CS1 module remain higher by a factor of 3 to 7 compared to the ITER CS3U and CS3L modules, respectively. It is to be noted that while in ITER coupling and magnetization losses are comparable over the pulse, in DEMO the losses are predominantly hysteretic. This behavior is a direct consequence of the high aspect ratio of the coated conductors, which strongly influences the magnetization behavior and leads to significantly higher hysteretic losses.

5. Conclusion

This study evaluated the instantaneous power losses in sector-shaped, twisted-stacked HTS cables within a simplified plasma scenario for the EU-DEMO central solenoid (CS) module. The analysis focused on both magnetization and coupling losses, using a novel analytical model to predict the power dissipation in the HTS stacks. The results clearly indicate that magnetization losses are significantly higher than coupling losses, with a ratio that varies between 2 and 500, depending on the plasma scenario phase. By integrating over the reference scenario, the magnetization losses are approximately 4.2 times greater than coupling losses, highlighting a significant technological challenge for the use of HTS in fusion magnets.

Furthermore, a comparison with calculations traditionally used for low-temperature superconducting conductors, such as those applied in the ITER project, shows that the HTS conductor losses behave similarly to a composite material with filaments having a diameter equal to the tape width.

Although the coupling losses are currently underestimated, one approach to reduce these losses would be to adjust the ramp rates during specific phases, such as the plasma current ramp-up (PCRU) and the current ramp-down (CRD). For magnetization losses, strategies like modifying the aspect ratio of the tapes or employing striated tapes could significantly reduce power dissipation, offering potential solutions for future HTS conductor designs in fusion applications.

In conclusion, while HTS conductors is promising for use in fusion magnets, further research is needed to optimize the designs and mitigate the high magnetization losses that currently represent a key challenge. Moreover, a more refined understanding of coupling losses during the plasma start-up and breakdown phases will be crucial for improving overall conductor efficiency.

As a final note, we would like to underline that this study primarily focuses on the total AC loss estimation rather than its spatial distribution within the coil. The current model is purely electromagnetic and does not account for thermal or thermo-hydraulic effects. However, we acknowledge that local concentrations of ac lossese could lead to thermal hotspots, which must be considered in the coil's cooling design. Future work will address this aspect by investigating localized loss distributions and their impact on thermal management, potentially through computational fluid dynamics (CFD) or finite element method (FEM) simulations.

CRediT authorship contribution statement

Gianluca De Marzi: Writing – original draft, Software, Methodology, Investigation, Formal analysis, Conceptualization. **Valentina Corato:** . **Monika Lewandowska:** Writing – review & editing, Methodology.

Declaration of competing interest

The authors declare that they have no known competing financial interests or personal relationships that could have appeared to influence the work reported in this paper.

Acknowledgements

This work has been carried out within the framework of the EUROfusion Consortium and has received funding from the Euratom Research and Training Programme 2021–2025 under Grant Agreement No. 101052200. Views and opinions expressed are however those of the author(s) only and do not necessarily reflect those of the European Union or the European Commission. Neither the European Union nor the European Commission can be held responsible for them.

The work was partially supported as the international project called 'PMW', co-financed by the Polish Ministry of Science and Higher Education within the framework of the scientific financial resources for 2024.

Data availability

Data will be made available on request.

References

[1] Meschini S, Laviano F, Ledda F, Pettinari D, Testoni R, Torsello D and Panella B 2023 Review of commercial nuclear fusion projects *Front Energy Res* **11**.
[2] Whyte DG, Minervini J, LaBombard B, Marmar E, Bromberg L, Greenwald M. Smaller & Sooner: Exploiting High Magnetic Fields from New Superconductors for a More Attractive Fusion Energy Development Path. *J Fusion Energ* 2016;35:41–53.
[3] Sarasola X, Wesche R, Ivashov I, Sedlak K, Uglietti D and Bruzzone P 2020 Progress in the Design of a Hybrid HTS-Nb3Sn-NbTi Central Solenoid for the EU DEMO *IEEE Transactions on Applied Superconductivity* **30**.
[4] Guarino R, Lewandowska M, Dembkowska A, Bykovskiy N, Sarasola X, Sedlak K. Thermal-hydraulic analysis of alternative cable-in-conduit conductors for the European DEMO hybrid central solenoid. *Fusion Eng Des* 2023;187:113368.
[5] Corato V, Vorpahl C, Sedlak K, Anvar V A, Bennet J, Biancolini M E, Bonne F, Bonifetto R, Boso D P, Brighenti A, Bruzzone P, Celentano G, della Corte A, De Marzi G, D'Auria V, Dembkowska A, Dicuonzo O, Zignani C F, Fietz W H, Frittitta C, Giannini L, Giorgetti F, Guarino R, Heller R, Hoa C, Huguet M, Jiolat G, Kumar M, Lacroix B, Lewandowska M, Misiara N, Morici L, Muzzi L, Nickel D S, Nicollet S, Nijhuis A, Nunio F, Portafaix C, Sarasola X, Savoldi L, Tiseanu I, Tomassetti G, Torre A, Turtù S, Uglietti D, Vallcorba R, Weiss K P, Wesche R, Wolf M J, Yagotintsev K, Zani L, Zanino R and Zappatore A 2022 The DEMO magnet system – Status and future challenges *Fusion Engineering and Design* **174**.
[6] Muzzi L, Augieri A, Celentano G, Chiarelli S, Della Corte A, De Marzi G, Di Zenobio A, Giannini L, Marchetti M, Masi A, Messina G, Rufoloni A, Turtu S, Vannozzi A, Bragagni A, Seri M, Arabi M, Anemona A and Formichetti A 2023 Design and Feasibility Assessment of an HTS Sector Shaped High-Current Conductor for Fusion Coils *IEEE Transactions on Applied Superconductivity* **33**.
[7] De Marzi G, Muzzi L, Grilli F. An analytical model for predicting the magnetization loss in HTS sector-shaped conductors for fusion. *Supercond Sci Technol* 2024;37:125007.
[8] Kovari M, Kemp R, Lux H, Knight P, Morris J, Ward DJ. "PROCESS": A systems code for fusion power plants—Part 1: Physics. *Fusion Eng Des* 2014;89:3054–69.
[9] Kovari M, Fox F, Harrington C, Kembleton R, Knight P, Lux H and Morris J 2016 "PROCESS": A systems code for fusion power plants – Part 2: Engineering *Fusion Engineering and Design* **104** 9–20.
[10] COMSOL Multiphysics® v. 5.4. www.comsol.com. COMSOL AB, Stockholm, Sweden.
[11] Wilson M N 1983 *Superconducting magnets* (Clarendon Press).
[12] Morgan GH. Theoretical Behavior of Twisted Multicore Superconducting Wire in a Time-Varying Uniform Magnetic Field. *J Appl Phys* 1970;41:3673–9.
[13] Carr WJ. ac loss in a twisted filamentary superconducting wire. I *J Appl Phys* 1974;45:929–34.
[14] Ries G. Ac-losses in multifilamentary superconductors at technical frequencies. *IEEE Trans Magn* 1977;13:524–6.
[15] Bauer P, Breschi M, Cavallucci L, Duchateau J L, Gauthier F, Torre A and Turck B 2022 Description of the AC Loss Model for the ITER Central Solenoid During a Plasma Scenario *IEEE Transactions on Applied Superconductivity* **32**.
[16] Torre A, Bauer P, Duchateau J L, Gauthier F and Turck B 2022 Review of Experimental Results and Models for AC Losses in the ITER PF and CS Conductors *IEEE Transactions on Applied Superconductivity* **32**.
[17] Ueno Y, Nagamoto N, Kawagoe A. OBANA T and TAKAYASU M. Evaluation AC Losses in Large-Scale Conductors Consisting of Stacked REBCO Tapes *Plasma and Fusion Research* 2021;16:2405071.
[18] Kim YB, Hempstead CF, Strnad AR. Critical Persistent Currents in Hard Superconductors. *Phys Rev Lett* 1962;9:306.
[19] Zhang X, Zhong Z, Ruiz HS, Geng J, Coombs TA. General approach for the determination of the magneto-angular dependence of the critical current of YBCO coated conductors. *Supercond Sci Technol* 2016;30:025010.
[20] Blatter G, Feigel'Man M V., Geshkenbein V B, Larkin A I and Vinokur V M 1994 Vortices in high-temperature superconductors *Rev Mod Phys* **66** 1125.
[21] Campbell AM. A general treatment of losses in multifilamentary superconductors *Cryogenics (Guildf)* 1982;22:3–16.
[22] Uglietti D, Kang R, Wesche R and Grilli F 2020 Non-twisted stacks of coated conductors for magnets: Analysis of inductance and AC losses.
[23] Lee M, Yoon M, Lee JK, Park S, Choi K, Kim WS. Analysis of Magnetization Losses of Twisted Stacked-Tape Cables With Striated Strands. *IEEE Trans Appl Supercond* 2024;34:1–5.
[24] Amemiya N, Tominaga N, Toyomoto R, Nishimoto T, Sogabe Y, Yamano S, et al. Coupling time constants of striated and copper-plated coated conductors and the potential of striation to reduce shielding-current-induced fields in pancake coils. *Supercond Sci Technol* 2018;31:025007.
[25] Amemiya N, Kasai S, Yoda K, Jiang Z, Levin GA, Barnes PN, et al. AC loss reduction of YBCO coated conductors by multifilamentary structure. *Supercond Sci Technol* 2004;17:1464.
[26] Bauer P, Breschi M, Cavallucci L, Duchateau J L, Gauthier F, Ilyin Y, Schild T, Torre A and Turck B 2023 AC Losses Calculations for the ITER CS and PF Magnet Systems during Plasma Operation *IEEE Transactions on Applied Superconductivity* **33**.